CHEMISTRY
AN ASIAN JOURNAL

DOI: 10.1002/asia.201100472

# The Role of the nπ* $^1A_u$ State in the Photoabsorption and Relaxation of Pyrazine

**Chih-Kai Lin,*[a, b] Yingli Niu,[a] Chaoyuan Zhu,[a] Zhigang Shuai,[c, d] and Sheng Hsien Lin[a, b]**

**Abstract:** The geometric, energetic, and spectroscopic properties of the ground state and the lowest four singlet excited states of pyrazine have been studied by using DFT/TD-DFT, CASSCF, CASPT2, and related quantum chemical calculations. The second singlet nπ* state, $^1A_u$, which is conventionally regarded dark due to the dipole-forbidden $^1A_u \leftarrow {}^1A_g$ transition, has been investigated in detail. Our new simulation has shown that the state could be visible in the absorption spectrum by intensity borrowing from neighboring nπ* $^1B_{3u}$ and ππ* $^1B_{2u}$ states through vibronic coupling. The scans on potential-energy surfaces further indicated that the $^1A_u$ state intersects with the $^1B_{2u}$ states near the equilibrium of the latter, thus implying its participation in the ultrafast relaxation process.

**Keywords:** absorption · pyrazines · quantum chemistry · excited states · vibronic coupling

## Introduction

Pyrazine is a benchmark system in photochemistry that has been widely studied for more than half a century. Being a diazine molecule, this aromatic compound differs from benzene by substituting a pair of nitrogen atoms for carbon ones in the *para* position. The lone-pair electrons reside in the nonbonding orbitals of the nitrogen atoms and thus generate n–π* transitions in addition to π–π* ones upon excitation in the valence shell. In terms of symmetry, the ground state is designated as $S_0{}^1A_g$ of the $D_{2h}$ point group, and the lowest singlet nπ* and ππ* excited states have conventionally been assigned as $S_1{}^1B_{3u}$ and $S_2{}^1B_{2u}$, respectively.

The details in the ultraviolet absorption spectra of pyrazine were first resolved in solution in 1950s,[1] and the data from vapors were obtained in the following decades.[2–7] People found that the 325 nm absorption band, that is, the nπ* $^1B_{3u}$ state, has a lot of sharp peaks that have been assigned as $\nu_{6a}$ ($a_g$), $\nu_{9a}$ ($a_g$), $\nu_{10a}$ ($b_{1g}$) fundamentals and their overtones as well as combination bands.[3,4,6,7] The 265 nm band, that is, the ππ* $^1B_{2u}$ state, presents a distinctly different feature, which is quite intense and broad with few structures, though the crests could be assigned with the aid of the resonant Raman spectrum.[3] The significant difference in intensities between the two absorption bands indicates that the $^1B_{2u} \leftarrow {}^1A_g$ transition is strongly dipole-allowed, whereas the $^1B_{3u} \leftarrow {}^1A_g$ one is just weakly allowed, and the appearance of odd-vibrational-quanta peaks of the non-totally-symmetric mode ($\nu_{10a}$ $b_{1g}$) in the $^1B_{3u}$ band reveals the "intensity borrowing" absorption through vibronic coupling. Moreover, the broad feature implies a quite short lifetime of the $^1B_{2u}$ state. The lifetimes of $^1B_{2u}$ and $^1B_{3u}$ states have been recorded as approximately 20 fs and approximately 22 ps, respectively, by using photoelectron spectra.[8–10] Succeeding researchers proposed an ultrafast $^1B_{2u} \rightarrow {}^1B_{3u}$ relaxation mechanism through conical intersection. Domcke and co-workers firstly carried out ab initio calculations combined with mathematical models to describe this internal conver-

[a] Dr. C.-K. Lin, Dr. Y. Niu, Prof. C. Zhu, Prof. S. H. Lin
Department of Applied Chemistry
National Chiao Tung University
Hsinchu 30010 (Taiwan)
Fax: (+886) 3-5723764
E-mail: ethene@gate.sinica.edu.tw

[b] Dr. C.-K. Lin, Prof. S. H. Lin
Institute of Atomic and Molecular Sciences
Academia Sinica
Taipei 10617 (Taiwan)

[c] Prof. Z. Shuai
Key Laboratory of Organic Optoelectronics and Molecular Engineering
Department of Chemistry
Tsinghua University
Beijing 100084 (P.R. China)

[d] Prof. Z. Shuai
Key Laboratory of Organic Solids
Beijing National Laboratory for Molecular Science
Institute of Chemistry
Chinese Academy of Sciences
Beijing 100190 (P.R. China)

sion process and simulated the absorption spectra.[11–16] More recently, Werner and Suzuki et al. carried out dynamical simulation on related states, thus providing insights into the relaxation of the $^1B_{2u}$ state.[9,10,17,18] Islampour calculated the strength of vibronic coupling and the relaxation-rate constant using vibronic Hamiltonian matrix.[19] Lin and coworkers simulated the absorption spectra based on Fermi's golden rule with Franck–Condon factors;[20,21] they neglected the explicit contribution of conical intersection but still obtained good results consistent with experiments.

It should be noted that there are two nitrogen atoms with nonbonding orbitals, so the excitation of an n electron to the lowest π* orbital should be described by the linear combination of two equivalent configurations. It results in a pair of singlet nπ* states, $^1B_{3u}$ and $^1B_{2g}$. The former is more stable than the latter evaluated by the overlap integral of corresponding orbitals from a valence-bond scheme.[22] In a similar fashion, the excitation from n to the second-lowest π* generates $^1A_u$ and $^1B_{1g}$ states. All these nπ* states except $^1B_{3u}$ are regarded as "dark" since the transitions are dipole-forbidden by symmetry. Nevertheless, they might not be completely invisible from the absorption spectrum because of possible vibronic couplings with the neighboring intensely dipole-allowed ππ* $^1B_{2u}$ state. Furthermore, all of these nπ* states would probably participate in the relaxation mechanism of the ππ* $^1B_{2u}$ state as indicated by a recent dynamical simulation.[17]

The relative positions of these low-lying singlet excited states, in terms of energy, is therefore an important topic and has been investigated by various quantum chemical calculations including density functional theories (DFT) and their time-dependent (TD-DFT) components, configuration interaction singles (CIS), complete active-space self-consistent field (CASSCF) and that with the second-order Møller–Plesset perturbation (CASPT2), equation-of-motion coupled-cluster singles and doubles (EOM-CCSD), and so on.[23–25] It was found that the nπ* $^1B_{3u}$ state is unambiguously the lowest one, followed by the ππ* $^1B_{2u}$ state. Among the other nπ* states, $^1A_u$ lies close to, whereas $^1B_{2g}$ and $^1B_{1g}$ locate somewhat higher than, the $^1B_{2u}$ state. Compared with spectroscopic observations,[26–28] TD-DFT, CASPT2, and EOM-CCSD yielded generally small errors in excitation energies, whereas CIS and CASSCF showed apparent overestimations for some of these states.

The nπ* $^1A_u$ state, noted as the $S_3$ state in some literature reports, is of special interest because it was predicted by CASPT2 and TD-DFT to be lying between conventional $S_1$ $^1B_{3u}$ and $S_2$ $^1B_{2u}$ states.[25] To avoid confusion among state sequences, we skip the $S_n$ notation hereafter. As the $^1A_u$ state might no longer be dark through vibronic coupling, it should contribute to the absorption band located between $^1B_{3u}$ and $^1B_{2u}$ peaks, most likely the weak broad feature around 290 to 310 nm.[3,6] In this work, we have constructed the mathematical framework of vibronic couplings between these low-lying singlet excited states, carried out quantum chemical calculations on geometric optimizations, vibrational frequencies, potential-energy surfaces (PES) scans as well as vibronic coupling constants, and simulated the absorption spectrum that covers the range of all three states. In addition to the harmonic oscillator approximation, we have adopted the double-well potential model to describe certain vibrational modes.[13,29] The combination of computed adiabatic potentials and mathematical treatments on vibronic couplings could readily reveal the role of the $^1A_u$ state in the photoabsorption and relaxation processes.

## Theories

In general, the one-photon absorption cross section of a single molecule can be expressed by Fermi's golden rule [Eq. (1)]:[30–33]

$$\sigma(\omega) = \frac{4\pi^2\omega}{3\hbar c}\sum_{\{v_j\}}\sum_{\{v'_j\}} P_{a\{v_j\}}\left|\left\langle \Psi_{b\{v'_j\}}\left|\hat{\boldsymbol{\mu}}\right|\Psi_{a\{v_j\}}\right\rangle\right|^2 \delta\left(\omega_{b\{v'_j\},a\{v_j\}} - \omega\right) \quad (1)$$

in which $a$ and $b$ indicate the initial and final electronic states, $\{v_j\}$ and $\{v'_j\}$, are the corresponding vibrational quantum numbers, $\hat{\boldsymbol{\mu}}$ is the dipole moment operator, and $P_{a\{v_j\}}$ is the Boltzmann distribution function for the initial vibrational states. The values $\omega_{b\{v'_j\},a\{v_j\}}$ and $\omega$ refer to the energy gap between the two states and the excited energy (in the form of angular frequency), respectively. The value $\delta(\Delta\omega)$ represents the Dirac delta function, which is in practice substituted by the Lorentzian function or the Gaussian function under homogeneous or inhomogeneous dephasing.

According to the Born–Oppenheimer adiabatic approximation, the molecular wavefunction can be approximately defined by the direct product of electronic and vibrational parts, that is, $\Psi(\mathbf{r},\mathbf{Q}) = \Phi(\mathbf{r};\mathbf{Q})\Theta(\mathbf{Q})$ in which $\mathbf{r}$ denotes the electronic coordinates, and $\mathbf{Q}$ is the dimensionless normal-mode coordinate matrix that can be transformed from the Cartesian displacement coordinates $\mathbf{x}$ [Eq. (2)]:

$$\mathbf{Q} = \hbar^{-1/2}\boldsymbol{\omega}^{1/2}\mathbf{L}^{-1}\mathbf{M}^{1/2}\mathbf{x} \quad (2)$$

Here $\boldsymbol{\omega}^{1/2}$ and $\mathbf{M}^{1/2}$ are diagonal matrices, the elements of which are square roots of vibrational angular frequencies and atomic masses, respectively. The columns in $\mathbf{L}$ represent the eigenstates of the Hessian matrix.

The electronic wavefunction $\Phi(\mathbf{r};\mathbf{Q})$ is dependent on $\mathbf{Q}$ parametrically, and it can be expanded around a reference geometry $\mathbf{Q}_0$ based on the Herzberg–Teller expansion [e.g., Eq. (3)]:

$$\left|\Phi_a(\mathbf{Q})\right\rangle = \left|\Phi_a^0\right\rangle + \sum_{c\neq a} a_{ac}\left|\Phi_c^0\right\rangle = \left|\Phi_a^0\right\rangle + \sum_{c\neq a}\frac{H'_{ca}}{E_a^0 - E_c^0}\left|\Phi_c^0\right\rangle \quad (3)$$

in which $\Phi^0$ and $E^0$ refer to the eigenfunction and the eigenstate energy, respectively, of the electronic Schrödinger equation at the reference geometry $\mathbf{Q}_0$, and $H'$ denotes the

  

vibronic coupling matrix elements with the following definition [Eq. (4)]:

$$H'_{ca} = \left\langle \Phi_c^0 \left| \sum_i \left( \frac{\partial V}{\partial Q_i} \right)_0 \right| \Phi_a^0 \right\rangle Q_i = \sum_i \lambda_i^{ca} Q_i \qquad (4)$$

In the above equation, $V$ represents the electrostatic potential and $\lambda_i^{ca}$ is the vibronic coupling constant between states $a$ and $c$ with respect to the normal coordinate $Q_i$. The transition matrix element in Equation (1) can be rewritten as Equation (5):

$$\left\langle \Psi_{b\{v'_j\}} \left| \hat{\mu} \right| \Psi_{a\{v_j\}} \right\rangle = \left\langle \Theta_{b\{v'_j\}} \left| \mu_{ba}(\mathbf{Q}) \right| \Theta_{a\{v_j\}} \right\rangle \qquad (5)$$

in which $\mu_{ba}(\mathbf{Q}) \equiv \left\langle \Phi_b \left| \hat{\mu} \right| \Phi_a \right\rangle$ is the coordinate-dependent transition dipole moment vector. With expansion up to the second order [Eq. (6)]:

$$\mu_{ba}(\mathbf{Q}) = \mu_{ba}^0 + \sum_i \left( \frac{\partial \mu_{ba}}{\partial Q_i} \right)_0 Q_i + \frac{1}{2} \sum_{ij} \left( \frac{\partial^2 \mu_{ba}}{\partial Q_i \partial Q_j} \right)_0 Q_i Q_j \qquad (6)$$

in which $\boldsymbol{\mu}_{ba}^0$ is the zeroth-order transition dipole moment at the reference geometry $\mathbf{Q}_0$, whereas the first and second derivatives are [Eqs. (7) and (8)]:

$$\boldsymbol{\mu}_{ba}^{(i)} \equiv \left( \frac{\partial \boldsymbol{\mu}_{ba}}{\partial Q_i} \right)_0 = \sum_{c \neq a} \frac{\boldsymbol{\mu}_{bc}^0 \lambda_i^{ca}}{E_a^0 - E_c^0} + \sum_{c \neq b} \frac{\lambda_i^{bc} \boldsymbol{\mu}_{ca}^0}{E_b^0 - E_c^0} \qquad (7)$$

$$\boldsymbol{\mu}_{ba}^{(i,k)} \equiv \left( \frac{\partial^2 \boldsymbol{\mu}_{ba}}{\partial Q_i \partial Q_k} \right)_0 = 2 \sum_{c \neq a} \sum_{c' \neq b} \frac{\lambda_i^{bc'} \boldsymbol{\mu}_{c'c}^0 \lambda_k^{ca}}{\left( E_a^0 - E_c^0 \right) \left( E_b^0 - E_{c'}^0 \right)} \qquad (8)$$

Supposing the Duschinsky rotation effect is insignificant and the second-order term is negligible, Equation (5) becomes Equation (9):

$$\begin{aligned} \left\langle \Psi_{b\{v'_j\}} \left| \hat{\mu} \right| \Psi_{a\{v_j\}} \right\rangle &= \mu_{ba}^0 \left\langle \Theta_{b\{v'_j\}} \middle| \Theta_{a\{v_j\}} \right\rangle + \sum_i \mu_{ba}^{(i)} \left\langle \Theta_{b\{v'_j\}} \middle| Q_i \middle| \Theta_{a\{v_j\}} \right\rangle \qquad (9) \\ &= \mu_{ba}^0 \prod_j \left\langle \chi_{v'_j} \middle| \chi_{v_j} \right\rangle + \sum_i \frac{1}{\sqrt{2}} \mu_{ba}^{(i)} \left\{ \sqrt{v_i + 1} \left\langle \chi_{v'_i} \middle| \chi_{v_i+1} \right\rangle + \sqrt{v_i} \left\langle \chi_{v'_i} \middle| \chi_{v_i-1} \right\rangle \right\} \prod_{j \neq i} \left\langle \chi_{v'_j} \middle| \chi_{v_j} \right\rangle \end{aligned}$$

For clarity, Equation (1) at zero temperature is divided into three parts [Eq. (10)]:

$$\sigma(\omega) = \sigma^{\mathrm{FC}}(\omega) + \sigma^{\mathrm{FC/HT}}(\omega) + \sigma^{\mathrm{HT}}(\omega) \qquad (10)$$

in which [Eqs. (11) and (12)]:

$$\sigma^{\mathrm{FC}}(\omega) \equiv \frac{4\pi^2 \omega}{3\hbar c} \sum_{\{v'_j\}} \left| \boldsymbol{\mu}_{ba}^0 \right|^2 \prod_j \left| \left\langle \chi_{v'_j} \middle| \chi_{0_j} \right\rangle \right|^2 \delta\left( \omega_{b\{v'_j\},a\{0_j\}} - \omega \right) \qquad (11)$$

$$\sigma^{\mathrm{FC/HT}}(\omega) \equiv \frac{4\pi^2 \omega}{3\hbar c} \sum_i \sum_{\{v'_j\}} \boldsymbol{\mu}_{ba}^0 \cdot \boldsymbol{\mu}_{ab}^{(i)} \left[ \left\langle \chi_{v'_i} \middle| \chi_{1_i} \right\rangle \left\langle \chi_{v'_i} \middle| \chi_{0_i} \right\rangle \prod_{j \neq i} \left| \left\langle \chi_{v'_j} \middle| \chi_{0_j} \right\rangle \right|^2 \right] \delta\left( \omega_{b\{v'_j\},a\{0_j\}} - \omega \right) \qquad (12)$$

and [Eq. (13)]:

$$\begin{aligned} \sigma^{\mathrm{HT}}(\omega) \equiv{}& \frac{4\pi^2 \omega}{3\hbar c} \sum_{i,k} \sum_{\{v'_j\}} \frac{1}{2} \boldsymbol{\mu}_{ba}^{(i)} \cdot \boldsymbol{\mu}_{ab}^{(k)} \qquad (13) \\ &\times \left[ \left\langle \chi_{0_i} \middle| \chi_{v'_i} \right\rangle \left\langle \chi_{v'_i} \middle| \chi_{1_i} \right\rangle \left\langle \chi_{1_k} \middle| \chi_{v'_k} \right\rangle \left\langle \chi_{v'_k} \middle| \chi_{0_k} \right\rangle \prod_{j \neq i,k} \left| \left\langle \chi_{v'_j} \middle| \chi_{0_j} \right\rangle \right|^2 \right] \delta\left( \omega_{b\{v'_j\},a\{0_j\}} - \omega \right) \end{aligned}$$

The vibronic coupling constant $\lambda_i$ can be estimated based on the method proposed by Domcke et al.[13,15] Briefly, the potentials of two interacting electronic states $b$ and $c$ are described by Equation (14):

$$\mathbf{V}(Q_i) = \frac{1}{2} \omega_i Q_i^2 \mathbf{1} + \begin{pmatrix} \Delta E_b + \gamma_i^b Q_i^2 & \lambda_i^{bc} Q_i \\ \lambda_i^{bc} Q_i & \Delta E_c + \gamma_i^c Q_i^2 \end{pmatrix} \qquad (14)$$

in which $\Delta E$ is the vertical excitation energy. The $\lambda_i^{bc}$ value as well as the $\gamma_i^{b,c}$ parameters can be fitted following a PES scan along the coupling coordinate $Q_i$.

Now consider the transitions from 0) $^1A_g$ ground state to 1) $^1B_{3u}$, 2) $^1B_{2u}$, and 3) $^1A_u$ excited states of pyrazine in the $D_{2h}$ point group. The $^1A_u \leftarrow {}^1A_g$ transition is dipole-forbidden, which means that $\boldsymbol{\mu}_{30}^0$ is zero at the ground-state equilibrium and hence both $\sigma^{\mathrm{FC}}(\omega)$ and $\sigma^{\mathrm{FC/HT}}(\omega)$ are zero. However, the first derivative $\boldsymbol{\mu}_{30}^{(i)}$ could be nonzero by intensity borrowing from neighboring $^1B_{3u} \leftarrow {}^1A_g$ and $^1B_{2u} \leftarrow {}^1A_g$ transitions, in which $\boldsymbol{\mu}_{10}^0$ and $\boldsymbol{\mu}_{20}^0$ are nonzero, through vibronic coupling of mode $i$, the $\lambda_i^{31}$ or $\lambda_i^{32}$ values of which are nonzero. As a result, the most contribution comes from the diagonal terms of $\sigma^{\mathrm{HT}}(\omega)$ [Eq. (15)]:

$$\sigma_{ii}^{\mathrm{HT}}(\omega) \equiv \frac{4\pi^2 \omega}{3\hbar c} \sum_{\{v'_j\}} \frac{1}{2} \left| \boldsymbol{\mu}_{30}^{(i)} \right|^2 \left[ \left| \left\langle \chi_{v'_i} \middle| \chi_{1_i} \right\rangle \right|^2 \prod_{j \neq i} \left| \left\langle \chi_{v'_j} \middle| \chi_{0_j} \right\rangle \right|^2 \right] \delta\left( \omega_{3\{v'_j\},0\{0_j\}} - \omega \right) \qquad (15)$$

The $^1B_{3u} \leftarrow {}^1A_g$ transition is weakly dipole-allowed, and therefore $\sigma^{\mathrm{FC}}(\omega)$ is nonzero yet not large. The value of $\sigma^{\mathrm{HT}}(\omega)$ is also nonzero through vibronic coupling, but the cross-term $\sigma^{\mathrm{FC/HT}}(\omega)$ is zero due to the orthogonality of dipole moment components within this four-state framework. The $^1B_{2u} \leftarrow {}^1A_g$ transition, on the other hand, is strongly dipole-allowed, and consequently $\sigma^{\mathrm{FC}}(\omega)$ dominates.

  

## Computational Methods

To investigate the properties of relevant electronic states of pyrazine, we have carried out both DFT and ab initio calculations. In the DFT approach, B3LYP and B971 functionals were applied for the geometric optimization and vibrational modes of the $^1A_g$ ground state, and their time-dependent components (TD-DFT) were used to describe the excitation energies, transition dipole moments, and geometric properties of the low-lying singlet excited states. Results from the two functionals were found to be quite similar. In the ab initio category, CASSCF (or CAS for short) and CASPT2 in the state-average manner were applied. Several different-sized active spaces were tested, and it turned out that the (10,8) one—that is, ten electrons in six valence π orbitals plus two nonbonding orbitals—was adequate for computing structures and transition energies under the native $D_{2h}$ point group of pyrazine.[25] CIS with the perturbative doubles [CIS(D)] was also applied to compare vertical excitation energies. In addition to equilibrium geometries, conical intersection points were searched by CASSCF to deduce vibronic couplings between neighboring electronic states.

The Pople-type 6-311++G(d,p) and the Dunning-type aug-cc-pVTZ basis sets were used in this work. The two basis sets turned out to make minor differences, and hence only results from the former are shown. DFT and TD-DFT calculations were carried out with Gaussian 09,[34] whereas CASSCF and CASPT2 ones were performed with MOLPRO 2006.[35]

## Results and Discussion

### Equilibrium Geometries and Excitation Energies

The optimized geometries of the ground state ($^1A_g$), the lowest three singlet nπ* excited states ($^1B_{3u}$, $^1A_u$, and $^1B_{2g}$), and the lowest singlet ππ* ($^1B_{2u}$) excited state of pyrazine computed by DFT/TD-DFT with the B3LYP functional, CASSCF(10,8), and CASPT2(10,8) are listed in Table 1. To the best of our knowledge, this is the first report that concerns the equilibrium geometries of the optically dark $^1A_u$ and $^1B_{2g}$ states. Focusing on the $^1A_u$ state, the data shows that the C–C bond length becomes noticeably longer and the C–N–C angle is apparently larger than other states, whereas the C–N bond length somewhat contracts. The overall effect is a significant expansion of the aromatic ring. According to the molecular orbital maps and excitation coefficients calculated by TD-DFT as shown in Figure 1 and Table 2, the $^1A_u$ state has a major configuration of the HOMO→LUMO+1 transition in which the nonbonding electron enters the C–N-bonding/C–C-antibonding orbital and results in the ring deformation.

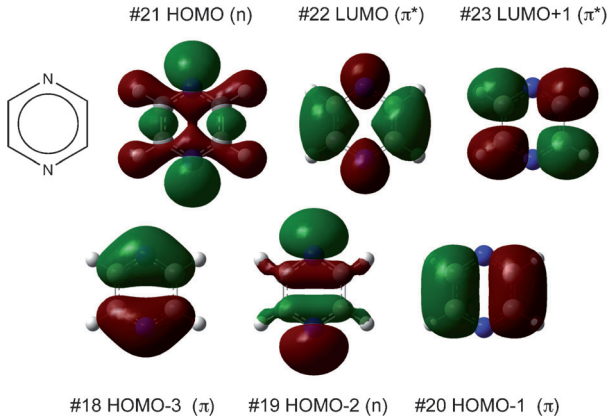


Figure 1. Selected molecular orbital maps of pyrazine calculated by DFT/B3LYP. HOMO and HOMO−2 show the nonbonding character, HOMO−1 and HOMO−3 are π bonding, and LUMO and LUMO+1 are π* antibonding.

The vertical (Franck–Condon) and the adiabatic (0–0 transition) energies from the ground state to these low-lying singlet states are listed in Table 3. At the Franck–Condon point, it is clear that $^1B_{3u}$ is the lowest and $^1B_{2g}$ is the highest among the four states studied both experimentally and computationally. The results of TD-DFT and CASPT2 in this

Table 1. Optimized geometries of pyrazine in its ground state and the lowest four singlet excited states. The bond lengths ($r$) are in Å and the angles ($\theta$) in degrees. All structures belong to the $D_{2h}$ point group.

| State | Method | $r_{CN}$ | $r_{CC}$ | $r_{CH}$ | $\theta_{CNC}$ | $\theta_{NCC}$ | $\theta_{NCH}$ |
|---|---|---|---|---|---|---|---|
| ground $^1A_g$ | B3LYP | 1.335 | 1.395 | 1.086 | 116.0 | 122.0 | 117.2 |
| | CASSCF | 1.329 | 1.395 | 1.075 | 116.1 | 122.0 | 117.2 |
| | CASPT2 | 1.343 | 1.402 | 1.086 | 115.0 | 122.5 | 116.9 |
| | calcd[a] | 1.346 | 1.402 | 1.085 | 115.6 | 122.3 | 117.5 |
| | exp[b] | 1.338 | 1.397 | 1.083 | 115.7 | 122.2 | 117.9 |
| nπ* $^1B_{3u}$ | TD-B3LYP | 1.343 | 1.396 | 1.084 | 120.0 | 120.0 | 120.5 |
| | CASSCF | 1.353 | 1.383 | 1.072 | 119.6 | 120.2 | 119.5 |
| | CASPT2 | 1.348 | 1.409 | 1.085 | 119.5 | 120.3 | 120.7 |
| | calcd[c] | 1.357 | 1.387 | 1.073 | 119.3 | 120.3 | 119.4 |
| ππ* $^1B_{2u}$ | TD-B3LYP | 1.367 | 1.428 | 1.086 | 110.2 | 124.9 | 116.6 |
| | CASSCF | 1.368 | 1.432 | 1.073 | 112.2 | 123.9 | 116.8 |
| | CASPT2 | 1.376 | 1.439 | 1.086 | 110.4 | 124.8 | 116.6 |
| | calcd[d] | 1.392 | 1.428 | 1.067 | 113.9 | 123.1 | 116.7 |
| nπ* $^1A_u$ | TD-B3LYP | 1.299 | 1.505 | 1.081 | 127.3 | 116.4 | 122.7 |
| | CASSCF | 1.302 | 1.489 | 1.070 | 126.6 | 116.7 | 122.0 |
| | CASPT2 | 1.309 | 1.510 | 1.083 | 126.7 | 116.6 | 122.9 |
| nπ* $^1B_{2g}$ | TD-B3LYP | 1.381 | 1.349 | 1.082 | 125.8 | 117.1 | 116.9 |
| | CASSCF | 1.387 | 1.347 | 1.071 | 123.4 | 118.3 | 117.0 |
| | CASPT2 | 1.387 | 1.361 | 1.083 | 124.2 | 117.9 | 116.9 |

[a] MP2/DZP.[15] [b] From electron diffraction and liquid-crystal NMR spectroscopy.[37] [c] CAS(10,8)/DZP.[38] [d] CAS(10,8)/3-21G.[39]

  

Table 2. Major excitation configurations to the lowest four singlet excited states at the ground-state equilibrium geometry calculated by TD-B3LYP.

| State | Major configuration | Coefficient |
|---|---|---|
| $n\pi^*\ ^1B_{3u}$ | #21 HOMO→#22 LUMO | 0.707 |
| $\pi\pi^*\ ^1B_{2u}$ | #20 HOMO−1→#22 LUMO | 0.664 |
| | #18 HOMO−3→#23 LUMO+1 | −0.239 |
| $n\pi^*\ ^1A_u$ | #21 HOMO→#23 LUMO+1 | 0.706 |
| $n\pi^*\ ^1B_{2g}$ | #19 HOMO−2→#22 LUMO | 0.704 |

Table 3. Vertical ($\Delta E_{FC}$) and adiabatic ($\Delta E_{ad}$) excitation energies [eV] from the ground state to the low-lying singlet excited states.

| State | $n\pi^*\ ^1B_{3u}$ | | $\pi\pi^*\ ^1B_{2u}$ | | $n\pi^*\ ^1A_u$ | | $n\pi^*\ ^1B_{2g}$ | |
|---|---|---|---|---|---|---|---|---|
| Excitation energy | $\Delta E_{FC}$ | $\Delta E_{ad}$ | $\Delta E_{FC}$ | $\Delta E_{ad}$ | $\Delta E_{FC}$ | $\Delta E_{ad}$ | $\Delta E_{FC}$ | $\Delta E_{ad}$ |
| TD-B3LYP | 3.94 | 3.83 | 5.40 | 5.18 | 4.61 | 3.87 | 5.57 | 4.98 |
| TD-B971 | 3.95 | 3.84 | 5.41 | 5.18 | 4.63 | 3.87 | 5.63 | 4.96 |
| CASSCF(10,8) | 4.87 | 4.72 | 5.11 | 4.84 | 5.90 | 5.22 | 5.93 | 5.29 |
| CASPT2(10,8) | 3.78 | 3.62 | 4.71 | 4.34 | 4.30 | 3.56 | 5.33 | 4.73 |
| CIS(D) | 4.47 | – | 5.49 | – | 4.86 | - | 6.38 | – |
| EOM-CCSD(T)[a] | 3.95 | – | 4.64 | – | 4.81 | – | 5.56 | – |
| exptl[b] | 3.94 | 3.83 | 4.81 | 4.69 | – | – | 5.50 | 5.46 |

[a] With the 6-31+G(d,p) basis set.[24] [b] From UV absorption and near-threshold electron energy-loss spectroscopy.[6,7,25,28]

work and EOM-CCSD(T) from a previous report[24] were generally consistent with experimental findings, whereas CASSCF and CIS(D) showed some overestimates. The relative positions of $^1B_{2u}$ and $^1A_u$, however, are not definite. CASSCF and EOM-CCSD(T) indicated that the latter locates higher than the former, whereas TD-DFT, CASPT2, and CIS(D) showed a reversed sequence. Moreover, TD-DFT and CASPT2 predicted that $^1A_u$ becomes nearly isoenergetic with $^1B_{3u}$ after relaxation to their equilibrium geometries (differed by only around 0.05 eV). Supposing this prediction to be correct, $^1A_u$ might play an important intermediate role in the $^1B_{2u}\rightarrow{}^1B_{3u}$ relaxation process by vibronic coupling with the two states. With a similar coupling mechanism, this dipole-forbidden state upon optical excitation should be no longer dark and probably reveals its contribution between $^1B_{3u}$ and $^1B_{2u}$ absorption bands. These points of view are explored and verified in the following PES scans and spectral simulations.

## Vibrational Modes and PES Scan

The vibrational frequencies of all relevant states have been calculated by different methods under the harmonic approximation as shown in Table 4. The Huang–Rhys factors of totally symmetric modes ($a_g$), defined as $S_i^{HR} \equiv (\Delta Q_i)^2/2$ in which $\Delta Q_i$ is the dimensionless displacement coordinate of mode $i$, calculated on the basis of DFT and CASSCF data, are listed in Table 5. The $\nu_{6a}$ mode, which is the totally symmetric mode with the lowest frequency, raises particular interest since it has a relatively large Huang–Rhys factor upon excitation to each state, thus implying a major component of spectral progression. It is also proposed as the major tuning mode in the ultrafast $^1B_{2u}\rightarrow{}^1B_{3u}$ relaxation mechanism because the crossing point between the two surfaces along the $Q_{6a}$ coordinate was estimated to be quite close to the $^1B_{2u}$ equilibrium.[13,15] For this reason, we carried out a PES scan

Table 4. Vibrational frequencies [$cm^{-1}$] of all 24 modes of pyrazine.

| Sym | Mode[a] | $^1A_g$ Exp[b] | DFT[c] | CAS[d] | CASPT2[d] | $n\pi^*\ ^1B_{3u}$ Exp[e] | TDDFT | CAS | $\pi\pi^*\ ^1B_{2u}$ TDDFT | CAS | $n\pi^*\ ^1A_u$ TDDFT | CAS | $n\pi^*\ ^1B_{2g}$ TDDFT | CAS |
|---|---|---|---|---|---|---|---|---|---|---|---|---|---|---|
| $a_g$ | $\nu_{6a}$ | 596 | 612 | 643 | 601 | 585 | 620 | 550 | 546 | 567 | 650 | – | 517 | 545 |
| | $\nu_1$ | 1015 | 1038 | 1074 | 1025 | 970 | 1024 | 1061 | 969 | 988 | 942 | 838 | 975 | 987 |
| | $\nu_{9a}$ | 1230 | 1253 | 1324 | 1261 | 1104 | 1195 | 1313 | 1237 | 1303 | 1195 | 1057 | 1208 | 1275 |
| | $\nu_{8a}$ | 1582 | 1614 | 1731 | 1622 | 1377 | 1534 | 1771 | 1532 | 1674 | 1417 | 1347 | 1665 | 1733 |
| | $\nu_2$ | 3055 | 3172 | 3351 | 3234 | – | 3196 | 3377 | 3175 | 3367 | 3225 | 3404 | 3214 | 3396 |
| $b_{1g}$ | $\nu_{10a}$ | 919 | 940 | 953 | 886 | 383 | 468 | 618 | 1158 | 681 | 338 | 342 | 821 | 789 |
| $b_{2g}$ | $\nu_4$ | 756 | 772 | 776 | 662 | 518 | 511 | 461 | 627 | 491 | 561 | 369 | 601 | 529 |
| | $\nu_5$ | 983 | 980 | 990 | 882 | 552 | 810 | 717 | 1034 | 749 | 585 | 528 | 874 | 886 |
| $b_{3g}$ | $\nu_{6b}$ | 704 | 720 | 758 | 710 | 662 | 688 | 701 | 659 | 702 | 659 | 679 | 659 | 699 |
| | $\nu_3$ | 1346 | 1373 | 1467 | 1377 | – | 1296 | 1440 | 1242 | 1428 | 1280 | 1403 | 931 | 1217 |
| | $\nu_{8b}$ | 1525 | 1578 | 1664 | 1564 | – | (588*i*) | 1664 | 1394 | 1590 | (640*i*) | – | 1353 | 1457 |
| | $\nu_{7b}$ | 3040 | 3151 | 3328 | 3215 | – | 3160 | 3353 | 3159 | 3348 | 3187 | 3337 | 3185 | 3371 |
| $a_u$ | $\nu_{16a}$ | 341 | 347 | 403 | 297 | 400 | 432 | 193 | 210 | 291 | 300 | 272 | 316 | 294 |
| | $\nu_{17a}$ | 960 | 989 | 995 | 832 | 743 | 824 | 772 | 911 | 807 | 787 | 646 | 870 | 866 |
| $b_{1u}$ | $\nu_{12}$ | 1021 | 1036 | 1114 | 1031 | – | 623 | 1002 | 970 | 992 | 761 | – | 923 | 950 |
| | $\nu_{18a}$ | 1136 | 1165 | 1225 | 1163 | – | 1012 | 1114 | 1096 | 1129 | 1141 | 1161 | 1371 | 1513 |
| | $\nu_{19a}$ | 1484 | 1511 | 1626 | 1515 | – | 1389 | 1553 | 1463 | 1551 | 1437 | 1508 | 1537 | 2439 |
| | $\nu_{13}$ | 3012 | 3152 | 3330 | 3216 | – | 3170 | 3355 | 3159 | 3349 | 3208 | 3375 | 3199 | 3424 |
| $b_{2u}$ | $\nu_{15}$ | 1063 | 1089 | 1041 | 1088 | – | 1079 | 1104 | 984 | 999 | 1157 | 1272 | 1112 | 1161 |
| | $\nu_{14}$ | 1149 | 1218 | 1150 | 1330 | – | 1267 | 1469 | 1280 | 1448 | 1459 | 1573 | 1249 | 1332 |
| | $\nu_{19b}$ | 1416 | 1440 | 1531 | 1445 | – | 1356 | 2003 | 1395 | 1876 | 820 | 799 | 1518 | 1572 |
| | $\nu_{20b}$ | 3063 | 3166 | 3346 | 3230 | – | 3193 | 3371 | 3172 | 3363 | 3214 | 3392 | 3207 | 3391 |
| $b_{3u}$ | $\nu_{16b}$ | 420 | 433 | 456 | 398 | 236 | 220 | 173 | (181*i*) | 250 | 445 | 385 | (74*i*) | 170 |
| | $\nu_{11}$ | 785 | 801 | 831 | 763 | 898 | 723 | 638 | 700 | 673 | 572 | 585 | 765 | 763 |

[a] Following assignments by McDonald and Rice[5] except that $\nu_{8a}$ and $\nu_{9a}$ are interchanged according to Innes et al.[7] and Domcke et al.[13,15] [b] From IR and Raman spectroscopy.[7] [c] With the B3LYP functional. [d] With the (10,8) active space. [e] From UV-absorption and threshold-ionization photoelectron spectroscopy.[5,40]

Table 5. Huang–Rhys factors of totally symmetric modes upon excitations from the $^1A_g$ ground state.

| Mode | $n\pi^*$ $^1B_{3u}$ TDDFT | CAS | $\pi\pi^*$ $^1B_{2u}$ TDDFT | CAS | $n\pi^*$ $^1A_u$ TDDFT | CAS | $n\pi^*$ $^1B_{2g}$ TDDFT | CAS |
|---|---|---|---|---|---|---|---|---|
| $\nu_{6a}$ | 0.616 | 0.698 | 1.866 | 0.925 | 1.667 | 1.828 | 6.350 | 4.305 |
| $\nu_1$ | 0.030 | 0.149 | 0.753 | 1.338 | 0.409 | 0.397 | 0.416 | 0.851 |
| $\nu_{9a}$ | 0.339 | 0.494 | 0.033 | 0.050 | 0.208 | 0.139 | 0.639 | 1.043 |
| $\nu_{8a}$ | 0.050 | 0.008 | 0.009 | 0.008 | 3.412 | 2.632 | 0.418 | 0.661 |
| $\nu_2$ | 0.004 | 0.003 | 0.001 | 0.004 | 0.027 | 0.023 | 0.018 | 0.013 |

along this coordinate around the ground-state equilibrium, similar to what was done by Domcke et al.,[13] yet we included more excited states in our TD-DFT and CASSCF/CASPT2 calculations.

The TD-DFT results are demonstrated in Figure 2 together with a comparison to previous HF/MP2 calculations.[13] The results of $^1A_g$, $^1B_{3u}$, and $^1B_{2u}$ states from both approaches are rather consistent. However, the previous

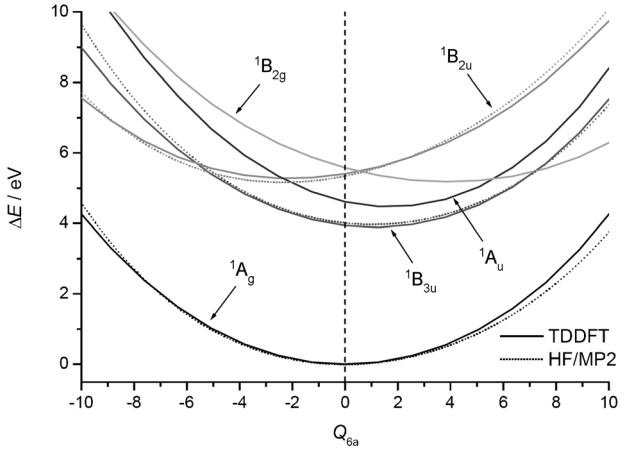


Figure 2. PES scan along the $Q_{6a}$ coordinate around the ground-state equilibrium by TD-DFT with the B3LYP functional (solid lines) in this work and by HF/MP2 (dotted lines) from a previous report.[13]

report did not consider more than three states. As expected from our geometric optimizations for excited states, the $^1A_u$ state locates between $^1B_{3u}$ and $^1B_{2u}$ at the Franck–Condon point ($Q_{6a}=0$). It is surprising that the intersection point between $^1A_u$ and $^1B_{2u}$ surfaces along this coordinate is even closer to the $^1B_{2u}$ bottom. In addition to $^1A_u$, the $^1B_{2g}$ potential also intersects $^1B_{2u}$ in the vicinity. It implies more than one relaxation channel after excitation to the $^1B_{2u}$ state; all the $^1B_{2u}\rightarrow{}^1B_{3u}$, $^1A_u$, and $^1B_{2g}$ processes should be competitive. This phenomenon was first predicted by Werner et al. in their dynamical simulation using TD-DFT,[17] but further consideration is still in demand.

The results from CASSCF and CASPT2 are illustrated in Figure 3. As mentioned above, CASSCF predicted higher energies for $^1A_u$ and $^1B_{2g}$ states, and in consequence their crossing points with $^1B_{2u}$ locate in an upper region. It could be a possible reason that Domcke and co-workers did not take these states into account. The CASPT2 data, on the

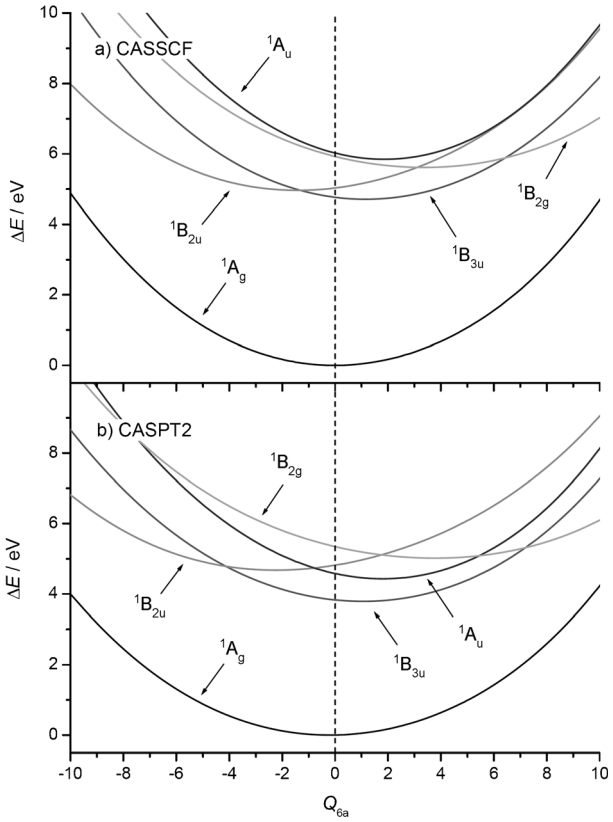


Figure 3. PES scan along the $Q_{6a}$ coordinate around the ground-state equilibrium by a) CASSCF and b) CASPT2.

other hand, possess a feature similar to TD-DFT. It points out again that $^1A_u$ and $^1B_{2g}$ states should be considered as well in the relaxation mechanism of the $^1B_{2u}$ state, which will be an important topic of our future work.

It was found that some vibrational modes showed imaginary frequencies, thereby suggesting the failure of the harmonic approximation for these modes. Taking the $\nu_{8b}$ ($b_{3g}$) mode of the $^1A_u$ state as an example shown in Figure 4, the

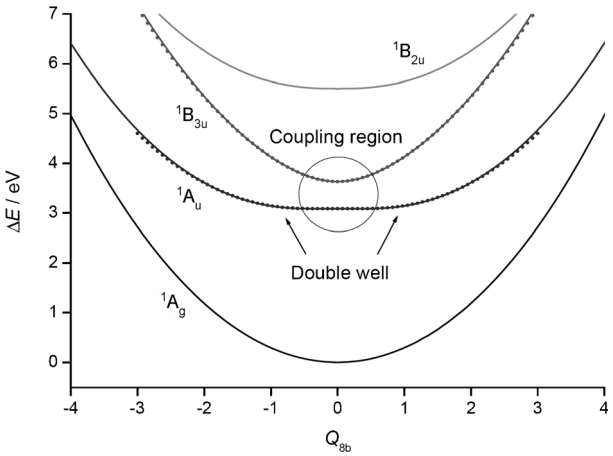


Figure 4. PES scan along the $\nu_{8b}$ double-well mode of the $^1A_u$ state by TD-DFT (solid lines) and fitting to coupling states (dotted lines) according to Equation (14).

  

TD-DFT PES scan revealed the mode to have a very shallow double-well potential instead of a harmonic one. It is the vibronic coupling between $^1B_{3u}$ and $^1A_u$ states through this $b_{3g}$ mode that distorts the shape of the two adiabatic potentials, thus making the lower one a double minimum.[29] Referring to Equation (14), the $\lambda_{8b}$ and $\gamma_{8b}$ values were fitted as 1930 and $-100\ cm^{-1}$, respectively. On the other hand, the double-well potential could be fitted in another way, say, the combinational of a quadratic potential and a Gaussian function [Eq. (16)]:

$$V(Q) = \frac{1}{2}\omega_0 Q^2 + A e^{-\alpha Q^2} + d \qquad (16)$$

This is a purely mathematical approach that is helpful in evaluating vibrational levels and Franck–Condon factors of the double well.[36] The fitting parameters and corresponding levels for the $\nu_{8b}$ mode of the $^1A_u$ state are listed in Table 6, which are utilized to simulate the absorption spectrum in the next section.

Table 6. Calculated potential parameters and vibrational levels of the $\nu_{8b}$ double-well mode of the $^1A_u$ state according to Equation (16).

| Potential parameters | | | | | |
|---|---|---|---|---|---|
| $\omega_0$ [$2\pi\,cm^{-1}$] | $A$ [$cm^{-1}$] | $\alpha$ | $d$ [$cm^{-1}$] | Barrier [$cm^{-1}$] | ZPE [$cm^{-1}$] |
| 1605 | 8303 | 0.6847 | 16406 | 622 | 472 |
| **Vibrational levels** | | | | | |
| $v'$ | 0 | 1 | 2 | 3 | 4 |
| $E_{v'}$ [$cm^{-1}$] | 0 | 1002 | 2102 | 3272 | 4494 |

## Absorption Spectra

The spectral shapes of the $^1B_{3u}$ and $^1B_{2u}$ absorption bands are quite different. The $^1B_{3u}$ band, beginning from around 325 nm and extending to around 300 nm, has a number of sharp peaks that are clearly assigned to $\nu_{6a}$ ($a_g$), $\nu_{9a}$ ($a_g$), $\nu_{10a}$ ($b_{1g}$), and so on, and their combinations.[3,4,6,7] The $^1B_{2u}$ band, by contrast, is rather broad and covers around 270 nm to around 230 nm with few fine structures.[3] Efforts on assigning peaks in this band have been made[3,7,21] and indicate the major components to be $\nu_1$ ($a_g$) and $\nu_{6a}$ ($a_g$), although most peaks are hidden in the broad feature, which is regarded an evidence of the ultrafast relaxation of the $^1B_{2u}$ state.[11–16] It is noteworthy that, in addition to the two distinct bands, there also exists a weaker broad character around 310 to 280 nm.[3,6] This does not seem to be just the tail of the $^1B_{3u}$ band, since the progressions in this band decay rather fast toward the higher-energy region.[6,15,20] Based on the knowledge of excited states calculated by TD-DFT and CASPT2 in this work as well as the prediction on relaxation dynamics by Werner et al.,[17] we have taken the $^1A_u$ state into account and made the first theoretical simulation on such an absorption feature. This dark $n\pi^*$ state may become visible through intensity borrowing from dipole-allowed transitions to neighboring states, thereby providing a suitable explanation for the weak broad band in the absorption spectrum.

Table 7. Vibronic coupling constants and derivatives of transition dipole moments between 0) $^1A_g$, 1) $^1B_{3u}$, 2) $^1B_{2u}$, and 3) $^1A_u$ states.

| Transition $b \leftarrow a$ | Coupling state $c$ | $\lvert\mu^0_{ca}\rvert$ [au] | $\lvert E^0_b - E^0_c\rvert$ [$cm^{-1}$] | Coupling mode $i$ | $\lambda_i^{bc}$ [$cm^{-1}$] | $\lvert\mu^{(i)}_{ba}\rvert$ [au] |
|---|---|---|---|---|---|---|
| 1 ($^1B_{3u}$)←0 ($^1A_g$) | 2 ($^1B_{2u}$) | 0.856 | 7660 | $\nu_{10a}$ ($b_{1g}$) | 1290[a] | 0.135 |
| 3 ($^1A_u$)←0 ($^1A_g$) | 1 ($^1B_{3u}$) | 0.242 | 5440 | $\nu_{6b}$ ($b_{3g}$) | 710 | 0.032 |
| | | | | $\nu_3$ ($b_{3g}$) | 840 | 0.037 |
| | | | | $\nu_{8b}$ ($b_{3g}$) | 1930 | 0.086 |
| | | | | $\nu_{7b}$ ($b_{3g}$) | 350 | 0.016 |
| 3 ($^1A_u$)←0 ($^1A_g$) | 2 ($^1B_{2u}$) | 0.856 | 2245 | $\nu_4$ ($b_{2g}$) | 790 | 0.301 |
| | | | | $\nu_5$ ($b_{2g}$) | 165 | 0.063 |

[a] Literature values: 1352 (CASSCF), 1472 (MRCI).[15]

As listed in Table 7, the zero-order transition dipole moment, $\mu^0_{ca}$, was calculated by using TD-DFT. The vibronic coupling constant, $\lambda_i^{bc}$, and the first derivative of transition moment, $\mu^{(i)}_{ba}$, between related states upon coupling coordinate $Q_i$ were calculated according to Equations (14) and (7), respectively. The absorption spectrum that covers the range from 330 to 230 nm was then simulated at zero temperature as shown in Figure 5. To compare this simulation with the experimental one,[3] the measured peak positions were

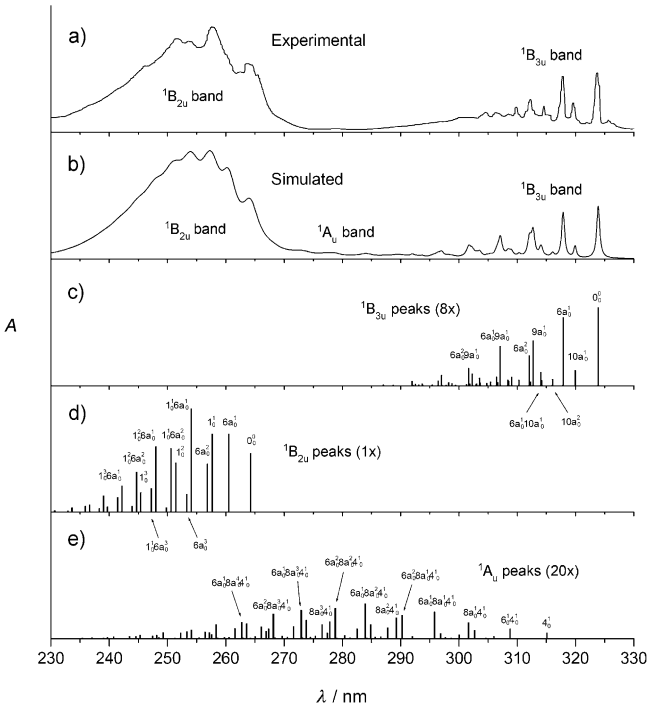


Figure 5. Absorption spectra of pyrazine covering $^1B_{3u}$, $^1B_{2u}$, and $^1A_u$ bands. a) Experimental UV spectroscopy.[3] b) Simulated spectrum with peaks broadened by homogeneous dephasing. c), d), and e) Calculated peak intensities and assignments in these bands.

adopted if applicable, whereas the peak intensities were estimated by transition dipole moments, vibronic couplings, and Franck–Condon factors obtained from first-principle calculations.

In the $^1B_{3u}$ absorption band, the major progressions composed of $\nu_{6a}$ ($a_g$) and $\nu_{9a}$ ($a_g$) are clearly seen. Both decrease monotonically as predicted by their Franck–Condon factors, the values of which are smaller than one (0.616 and 0.339, respectively, by TD-DFT). To fit experimental bandwidths, the homogeneous dephasing was set as 30 $cm^{-1}$ for the 0–0 transition and raised gradually as the vibrational energy increased. The appearance of the odd quantum peak of $\nu_{10a}$ ($b_{1g}$) represents the intensity-borrowing feature from the neighboring $^1B_{2u}$ state through vibronic coupling. This feature has been successfully reproduced by the simple Herzberg–Teller expansion described by Equation (15).

The dipole moment of the $^1B_{2u}\leftarrow{}^1A_g$ transition is about 3.5 times larger than that of the $^1B_{3u}\leftarrow{}^1A_g$ transition ($\boldsymbol{\mu}^0_{20}=0.856$ au and $\boldsymbol{\mu}^0_{10}=0.242$ au by TD-DFT), thus giving the total intensity of the $^1B_{2u}$ band to be one order higher than the $^1B_{3u}$ band. The major components of progressions in the $^1B_{2u}$ band are $\nu_{6a}$ ($a_g$) and $\nu_1$ ($a_g$). The bandwidth was set as 240 $cm^{-1}$ for the 0–0 transition and increased up to 400 $cm^{-1}$ for overtones and combination bands such as $1_0^3$ and $1_0^2 6a_0^2$ to reproduce the whole broad feature. In principle, $^1B_{2u}$ can also borrow intensity from $^1B_{3u}$ by vibronic coupling through $\nu_{10a}$, but the strength turned out to be too small relative to the direct transition to $^1B_{2u}$, thereby resulting in a negligible contribution overwhelmed in the broad band.

It is noticeable that some weak hot bands took place as the experimental spectra were not recorded under low-temperature conditions.[3,4,6] In the $^1B_{3u}$ band, there is a small absorption peak to the red of the 0–0 transition (Figure 5a) which has been assigned as $16b_1^1$.[4] In the $^1B_{2u}$ band, however, possible hot-band peaks should be embedded in the broad feature and thus indistinguishable. The overall contribution of hot bands was not significant and the temperature effect was therefore not considered further in the present simulated spectrum (Figure 5b).

The $^1A_u$ band is dipole-forbidden and thus must borrow intensity from either $^1B_{3u}$ or $^1B_{2u}$ to be visible. The vibronic coupling between $^1A_u$ and $^1B_{2u}$ occurs through $b_{2g}$ modes, among which $\nu_4$ is the major contributor. The coupling between $^1A_u$ and $^1B_{3u}$, on the other hand, requires $b_{3g}$ modes in which $\nu_{8b}$ plays the leading role (Table 7). Due to the large value of $\boldsymbol{\mu}^0_{20}$, the contribution from $^1A_u$-$^1B_{2u}$ coupling dominates this band. The progressions in this band are mainly composed of $\nu_{6a}$ ($a_g$) and $\nu_{8a}$ ($a_g$). The $\nu_{8a}$ series is relatively important and extends to the $^1B_{2u}$ region because of a large Huang–Rhys factor (3.412 by TD-DFT and 2.632 by CASSCF). As a result, the $^1A_u$ band presents a low-intensity but wide-range character, adequately filling the spectral window between the $^1B_{3u}$ and $^1B_{2u}$ bands. It shows, however, that our calculated $^1A_u$ band overestimates around 270 to 280 nm yet underestimates around 290 to 300 nm in critical comparison to the experimental spectrum. This may be attributed to possible inaccuracy of present computational results and should be examined with higher-level calculations in future works.

## Conclusion

In the present studies, the equilibrium geometries, vibrational frequencies, excitation energies, and vibronic couplings of the ground state ($^1A_g$) and the lowest four singlet excited states ($^1B_{3u}$, $^1B_{2u}$, $^1A_u$, and $^1B_{2g}$) of pyrazine have been calculated by DFT/TD-DFT, CASSCF, and CASPT2 methods. The $n\pi^*$ $^1A_u$ state was of particular concern because of its predicted location between $n\pi^*$ $^1B_{3u}$ and $\pi\pi^*$ $^1B_{2u}$ states. Although the $^1A_u\leftarrow{}^1A_g$ transition is dipole-forbidden, it can borrow the intensity from the $^1B_{2u}\leftarrow{}^1A_g$ and $^1B_{3u}\leftarrow{}^1A_g$ transitions through vibronic coupling. The $^1A_u$ absorption band therefore becomes slightly visible and covers the range between $^1B_{3u}$ and $^1B_{2u}$ bands, in agreement with experimental spectra. Furthermore, the existence of $^1A_u$ and $^1B_{2g}$ states in the vicinity of the $^1B_{2u}$ state and the locations of their conical intersections searched by PES scan reveal that these two optically dark states, in addition to the known bright $^1B_{3u}$ state, should be important in the ultrafast relaxation mechanism of the $^1B_{2u}$ state. The dynamic properties of these states will be the focus in our future work.


[1] F. Halverson, R. C. Hirt, *J. Chem. Phys.* **1951**, *19*, 711.
[2] M. Ito, R. Shimada, T. Kuraishi, W. Mizushima, *J. Chem. Phys.* **1957**, *26*, 1508.
[3] I. Suzuka, Y. Udagawa, M. Ito, *Chem. Phys. Lett.* **1979**, *64*, 333.
[4] Y. Udagawa, M. Ito, I. Suzuka, *Chem. Phys.* **1980**, *46*, 237.
[5] D. B. McDonald, S. A. Rice, *J. Chem. Phys.* **1981**, *74*, 4893.
[6] I. Yamazaki, T. Murao, T. Yamanaka, K. Yoshihara, *Faraday Discuss. Chem. Soc.* **1983**, *75*, 395.
[7] K. K. Innes, I. G. Ross, W. R. Moomaw, *J. Mol. Spectrosc.* **1988**, *132*, 492.
[8] V. Stert, P. Famanara, W. Radloff, *J. Chem. Phys.* **2000**, *112*, 4460.
[9] T. Horio, T. Fuji, Y.-I. Suzuki, T. Suzuki, *J. Am. Chem. Soc.* **2009**, *131*, 10392.
[10] Y.-I. Suzuki, T. Fuji, T. Horio, T. Suzuki, *J. Chem. Phys.* **2010**, *132*, 174302.
[11] R. Schneider, W. Domcke, *Chem. Phys. Lett.* **1988**, *150*, 235.
[12] M. Seel, W. Domcke, *J. Chem. Phys.* **1991**, *95*, 7806.
[13] L. Seidner, G. Stock, A. L. Sobolewski, W. Domcke, *J. Chem. Phys.* **1992**, *96*, 5298.
[14] G. Stock, W. Domcke, *J. Phys. Chem.* **1993**, *97*, 12466.
[15] C. Woywod, W. Domcke, A. L. Sobolewski, H.-J. Werner, *J. Chem. Phys.* **1994**, *100*, 1400.
[16] G. Stock, C. Woywod, W. Domcke, T. Swinney, B. S. Hudson, *J. Chem. Phys.* **1995**, *103*, 6851.
[17] U. Werner, R. Mitrić, T. Suzuki, V. Bonačić-Koutecký, *Chem. Phys.* **2008**, *349*, 319.
[18] U. Werner, R. Mitrić, V. Bonačić-Koutecký, *J. Chem. Phys.* **2010**, *132*, 174301.
[19] R. Islampour, M. Miralinaghi, *J. Phys. Chem. A* **2009**, *113*, 2340.
[20] R. X. He, C. Y. Zhu, C.-H. Chin, S. H. Lin, *Sci. China Ser. B* **2008**, *51*, 1166.
[21] R. X. He, C. Y. Zhu, C.-H. Chin, S. H. Lin, *Chem. Phys. Lett.* **2009**, *476*, 19.
[22] W. R. Wadt, W. A. Goddard, III, *J. Am. Chem. Soc.* **1975**, *97*, 2034.
[23] M. P. Fülscher, K. Andersson, B. O. Roos, *J. Phys. Chem.* **1992**, *96*, 9204.


  

[24] J. E. Del Bene, J. D. Watts, R. J. Bartlett, *J. Chem. Phys.* **1997**, *106*, 6051.
[25] P. Weber, J. R. Reimers, *J. Phys. Chem. A* **1999**, *103*, 9821.
[26] A. Bolovinos, P. Tsekeris, J. Philis, E. Pantos, G. Andritsopoulos, *J. Mol. Spectrosc.* **1984**, *103*, 240.
[27] Y. Okuzawa, M. Fujii, M. Ito, *Chem. Phys. Lett.* **1990**, *171*, 341.
[28] I. C. Walker, M. H. Palmer, *Chem. Phys.* **1991**, *153*, 169.
[29] P. Weber, J. R. Reimers, *J. Phys. Chem. A* **1999**, *103*, 9830.
[30] S. H. Lin, Y. Fujimura, H. J. Neusser, E. W. Schlag, *Multiphoton Spectroscopy of Molecules*, Academic Press, New York, **1984**, chapter 2.
[31] A. M. Mebel, M. Hayashi, K. K. Liang, S. H. Lin, *J. Phys. Chem. A* **1999**, *103*, 10674.
[32] K. K. Liang, R. Chang, M. Hayashi, S. H. Lin, *Principle of Molecular Spectroscopy and Photochemistry*, National Chung Hsing University Press, Taichung, **2001**, chapters 2 and 5.
[33] C.-K. Lin, M.-C. Li, M. Yamaki, M. Hayashi, S. H. Lin, *Phys. Chem. Chem. Phys.* **2010**, *12*, 11432.
[34] Gaussian 09, Revision A.02, M. J. Frisch, G. W. Trucks, H. B. Schlegel, G. E. Scuseria, M. A. Robb, J. R. Cheeseman, G. Scalmani, V. Barone, B. Mennucci, G. A. Petersson, H. Nakatsuji, M. Caricato, X. Li, H. P. Hratchian, A. F. Izmaylov, J. Bloino, G. Zheng, J. L. Sonnenberg, M. Hada, M. Ehara, K. Toyota, R. Fukuda, J. Hasegawa, M. Ishida, T. Nakajima, Y. Honda, O. Kitao, H. Nakai, T. Vreven, J. A. Montgomery, Jr., J. E. Peralta, F. Ogliaro, M. Bearpark, J. J. Heyd, E. Brothers, K. N. Kudin, V. N. Staroverov, R. Kobayashi, J. Normand, K. Raghavachari, A. Rendell, J. C. Burant, S. S. Iyengar, J. Tomasi, M. Cossi, N. Rega, J. M. Millam, M. Klene, J. E. Knox, J. B. Cross, V. Bakken, C. Adamo, J. Jaramillo, R. Gomperts, R. E. Stratmann, O. Yazyev, A. J. Austin, R. Cammi, C. Pomelli, J. W. Ochterski, R. L. Martin, K. Morokuma, V. G. Zakrzewski, G. A. Voth, P. Salvador, J. J. Dannenberg, S. Dapprich, A. D. Daniels, Ö. Farkas, J. B. Foresman, J. V. Ortiz, J. Cioslowski, D. J. Fox, Gaussian, Inc., Wallingford CT, **2009**.
[35] MOLPRO is a package of ab initio programs written by H.-J. Werner, P. J. Knowles, R. Lindh, F. R. Manby, P. Celani, T. Korona, G. Rauhut, R. D. Amos, A. Bernhardsson, A. Berning, D. L. Cooper, A. J. Dobbyn, F. Eckert, C. Hampel, G. Hetzer, A. W. Lloyd, S. J. McNicholas, W. Meyer, M. E. Mura, A. Nicklaß, P. Palmieri, R. Pitzer, U. Schumann, H. Stoll, R. Tarroni, T. Thorsteinsson, **2006**.
[36] C.-K. Lin, H.-C. Chang, S. H. Lin, *J. Phys. Chem. A* **2007**, *111*, 9347.
[37] S. Cradock, P. B. Liescheski, D. W. H. Rankin, H. E. Robertson, *J. Am. Chem. Soc.* **1988**, *110*, 2758.
[38] R. Berger, C. Fischer, M. Klessinger, *J. Phys. Chem. A* **1998**, *102*, 7157.
[39] A. L. Sobolewski, C. Woywod, W. Domcke, *J. Chem. Phys.* **1993**, *98*, 5627.
[40] L. Zhu, P. Johnson, *J. Chem. Phys.* **1993**, *99*, 2322.

Received: May 20, 2011
Published online: September 16, 2011

  